Biochimica et Biophysica Acta 1828 (2013) 213–222

Contents lists available at SciVerse ScienceDirect

Biochimica et Biophysica Acta

journal homepage: www.elsevier.com/locate/bbamem

The molecular organization of prenylated flavonoid xanthohumol in DPPC multibilayers: X-ray diffraction and FTIR spectroscopic studies

Marta Arczewska [a,1], Daniel M. Kamiński [a,b,1], Ewa Górecka [c], Damian Pociecha [c], Edward Rój [c], Adrianna Sławińska-Brych [d], Mariusz Gagoś [a,d,*]

[a] Department of Biophysics, University of Life Sciences in Lublin, Akademicka 13, 20-950 Lublin, Poland
[b] Department of Chemistry, University of Life Sciences in Lublin, Akademicka 15, 20-950 Lublin, Poland
[c] Fertilizers Research Institute, 24-110 Puławy, Poland
[d] Department of Cell Biology, Institute of Biology and Biotechnology, Maria Curie-Skłodowska University, 20-033 Lublin, Poland

ARTICLE INFO

Article history:
Received 2 June 2012
Received in revised form 3 October 2012
Accepted 11 October 2012
Available online 17 October 2012

Keywords:
DPPC multibilayers
Xanthohumol
Prenylated chalcone
ATR-FTIR
X-ray diffraction

ABSTRACT

Xanthohumol (XN) is the major prenylated flavonoid found in hop resin. It has attracted considerable attention in recent years due to its wide spectrum of biological activities and the beneficial effect on human health. Since lipid membrane is first target for biologically active compounds, we decided to investigate the influence of XN on the dipalmitoylphosphatidylcholine (DPPC) multibilayers. Interactions of XN with DPPC were investigated as a function of temperature and its concentration by using X-ray diffraction and the ATR-FTIR spectroscopy techniques. The aim of understanding the mechanisms of molecular interactions between XN and DPPC was to indicate the localization of the XN with respect to the membrane and the type of interaction with phospholipids. The results revealed that XN changes the physical properties of the DPPC multibilayers in the form of dry film. A new complex formation between XN and DPPC is reported. The detailed analysis of refraction effect indicates the changes in electron density ratio between hydrophobic and hydrophilic zones of lipid at phase transition. This is in compliance with reported changes in FTIR spectra where at pretransition XN moves from interface region between polar heads to the neighborhood of phosphate groups.

1. Introduction

The chalcone xanthohumol (2′,4′,6′,4-tetrahydroxy-3′-prenylchalcone; XN) is the major prenylated flavonoid found in hop resin (*Humulus lupulus*) [1]. In recent years, the number of studies have revealed that XN exhibits an interesting spectrum of pharmacological effects [2–6]. XN has attracted considerable interest because of its biological activities, including anticancer, antiangiogenic, anti-inflammatory, and antioxidative effects; it even inhibits HIV-1 induced cytopathic effects [4,7–13]. The anti-cancer activity of XN may be due in part to the inhibition of cytochrome P450 enzymes that activate carcinogens such as the heterocyclic amine 2-amino-3-methylimidazo (4,5-f) quinoline [12]. Xanthohumol (1–50 μM) suppressed tumor growth by inhibiting cell proliferation and inducing apoptosis in various carcinoma cells [7,14]. Unfortunately, the quantities of xanthohumol found in hop are too small to have any biological effects in normal consumption amounts [15]. Therefore, studies should be directed toward dietary supplements increasing xanthohumol content. Xanthohumol was first isolated by Power et al. [16] and its structure was later confirmed using partial synthesis and X-ray diffraction [17,18]. The XN molecule consists of two aromatic rings (A and B) substituted with hydroxyl and methoxyl groups, one α, β unsaturated double bond, and the prenyl unit [18,19], see the chemical structure in Scheme 1. The substitution of the flavonoid ring system with the prenyl unit and a $-OCH_3$ group increases the lipophilicity and confers the molecule a strong affinity for biological membranes [20]. Moreover, recent research has revealed that XN is responsible for the CETP (cholesteryl ester transfer protein) inhibitory activity via binding to CETP and/or the CETP–lipid complex [21]. The requirement of a 3-prenyl group seems to be necessary for the hydrophobic interaction between xanthohumol and the CETP–lipid complex.

Biological membranes play an important role in biomolecule transport, distribution, action, and selectivity. Therefore, it seems to be crucial to understand the molecular mechanism of their interaction with lipids in the model membrane. The effect of flavonoids on cell metabolism is well known, while the mechanism of their activity at the molecular level remains poorly elucidated and unclear. It was suggested that two relevant interactions of flavonoids with lipids are possible: (a) the partitioning in the non-polar core of the membrane, associated with the hydrophobic nature of the flavonoid; and (b) the interaction with the polar membrane interface depending on hydrogen bonding of the hydroxyl groups [22–24]. There is substantial evidence for the interactions of flavonoids with the lipid

* Corresponding author at: Department of Biophysics, University of Life Sciences in Lublin 20-950 Lublin, Poland. Tel.: +48 81 4456899; fax: +48 81 4456684.
E-mail address: mariusz.gagos@up.lublin.pl (M. Gagoś).
[1] Both authors contributed equally.

0005-2736/$ – see front matter © 2012 Elsevier B.V. All rights reserved.
http://dx.doi.org/10.1016/j.bbamem.2012.10.009

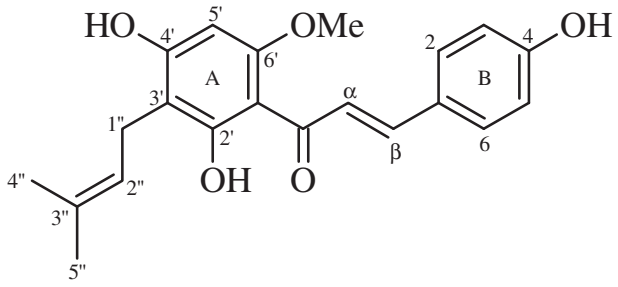

Scheme 1. The chemical structure of xanthohumol (XN).

membrane. The prediction of their localization in the lipid bilayer was investigated by NMR spectroscopy [25]. Moreover, differential scanning calorimetry (DSC) revealed a significant difference in the ability of flavonoids to modify lipid melting [26,27]. The well-documented quercetin may increase lipid viscosity because its molecules are supposed to be localized at the boundary between the polar and hydrophobic regions of the membrane and, consequently, its influence on the bilayer is comparable with that of cholesterol [28,29]. It was also suggested that flavonoids can influence the appearance and development of rafts or raft-like membrane domains in cellular membranes [30].

Despite many systematic studies about the flavonoid–lipid interaction, the influence of XN on the model membrane has not been discussed yet. Therefore, it seems important to elucidate the mechanisms responsible for XN–membrane interactions at the molecular level. The results obtained could provide useful knowledge on possible pharmacological applications of XN and valuable information for designing flavonoid-based drugs that will be important in modern medical research. The structure and NMR data of XN are described by Chadwick et al. [18]. However, there is no systematic X-ray study reported on XN in lipid multibilayer.

In the present paper, X-ray diffraction technique and ATR Fourier-transform infrared spectroscopy (ATR-FTIR) were applied to understand the membrane-associated biological activities of XN molecules.

The character of the mutual interactions between dipalmitoylphosphatidylcholine lipid (DPPC) and XN was discussed depending on its concentrations. The aim of the present study was to monitor the thermotropic phase behavior of DPPC multibilayers in the presence of XN concerning the configuration changes in different parts of the lipid molecules simultaneously by X-ray diffraction and ATR-FTIR measurements of the dry films. We have therefore been able to investigate the XN–DPPC interactions at the levels of the acyl chains, the carbonyl, the phosphate, and the choline groups. The XN effect on structural properties of DPPC multibilayers, in particular on the lipid packing and phase transition, can provide a much better understanding of the molecular interaction of XN with the biological membranes.

2. Materials and methods

Xanthohumol (XN) and dipalmitoylphosphatidylcholine (DPPC) were purchased from Sigma Chem. Co. (USA). The purity of the chemicals was 99%. All solvents were used without further purification.

2.1. Sample preparation

Multilamellar phospholipid vesicles (MLVs) were prepared using the standard procedure. To prepare the liposomes, 2 mg of DPPC was first dissolved in 0.5 ml chloroform inside chemical-resistant polypropylene centrifuge tube (Eppendorf) to obtain dry films. Xanthohumol was dissolved in methanol at the concentration of 4.0×10^{-3} M. To prepare xanthohumol containing liposomes, the required amount of XN from the stock solution was placed inside the sample tube with DPPC and mixed. The solution was then subjected to a stream of nitrogen to remove excess solvents. The remaining solvent was removed by evaporating the films in a vacuum dryer for 2 h. After complete solvent evaporation, 0.5 ml of ultrapure water was added and the mixture was homogenized with a sonicator (Bandelin Sonoplus) 3× for 1 s with 60% of total power.

The ATR-FTIR infrared absorption spectra were recorded on a 670-IR Varian spectrometer. Typically, 25 scans were collected at a resolution of 1 cm^{-1}. The liposome suspensions with XN were prepared according to the procedure described above and 200 μl of xanthohumol in different mole ratios in DPPC (1, 5, 10, 15, 20 and 50 mol%) spread on one surface of a Ge ATR crystal (face angle: 45°, 10 reflections, PIKE Technologies). The dry DPPC/XN films were prepared by evaporating the mixture under a stream of argon. The spectra of XN in DPPC in different mole ratios were performed in dry purified air (relative humidity, RH<5%, 31 °C). The spectra were recorded in a first heating cycle from 25 to 80 °C with 2−3 °C intervals and in second cycle from 39 to 102 °C. The up limit of temperature in the first cycle was chosen to prevent possible XN isomarization to isoxanthohumol [3] and DPPC decomposition. In second cycle probably a DPPC decomposition at high temperatures >90 °C was observed. The sample temperature was equilibrated for 2 min before acquisition of each spectrum. The RH of multibilayers during measurements was defined with reference to the main transition [31] of pure DPPC and was in the range of RH 1% ± 0.3 and 4.0% ± 0.5, see Fig. 1. Additionally, the amount of adsorbed water in multibilayers was monitored in situ using the water-adsorptivity parameter $A_{wr} = (A_w/A_{lt})$ defined as the ratio of the OH absorption band area (A_w) and the overall C−H stretching-vibration bands between ca. 2800 and ca. 3080 cm^{-1} (A_{lt}) [32].

The Ge crystal plate was cleaned with ultra pure organic solvents from Sigma-Aldrich. The spectral analysis was performed with Grams/AI software from ThermoGalactic Industries (USA). The deconvolution (Gaussian and Lorentzian) and curve fitting were analyzed by the peak-fitting module of OriginPro 8.6. The correlation coefficients for all fitted curves were higher than 0.998.

In the case of X-ray diffraction measurements the XN–DPPC mixture was deposited on the mica plates. Afterwards samples were left for 24 h in room temperature until complete water evaporation. Such prepared multibilayers were a subject of X-ray investigation.

2.2. X-ray measurements

X-ray diffraction patterns were collected with a Bruker D8 Discover system, working in the reflection mode. A parallel beam of CuKa radiation (line focus) was formed by Gebel mirror, and the diffracted intensity was controlled with a scintillation counter. Sample temperature was stabilized by the Anton Parr DCS350 heating stage (with accuracy 0.1 °C). Precision sample positioning was assured by the Eulerian cradle mounted on the goniometer.

The peak position and layer refraction were fitted with least square method. The errors were estimated from chi-square deviations. Before fitting the data were corrected for refraction effect according to the equation detailed presented in [33,34].

In this case the following parameters were fixed to: $d_1 = 20$ Å (thickness of hydrophilic refraction zone 1) and $n_1 = 0.999999$ (refraction index of zone 1). Only the parameter n_2 (refraction index of zone 2), scale factor and layer thickness d were free during fitting procedure. The refraction depends on this case on the ratio between refraction indices n_1 and n_2 thus the ratio n_1/n_2 is shown. The refraction indices change on the value 1×10^{-6} which is expected in the case of soft matter for X-ray diffraction.

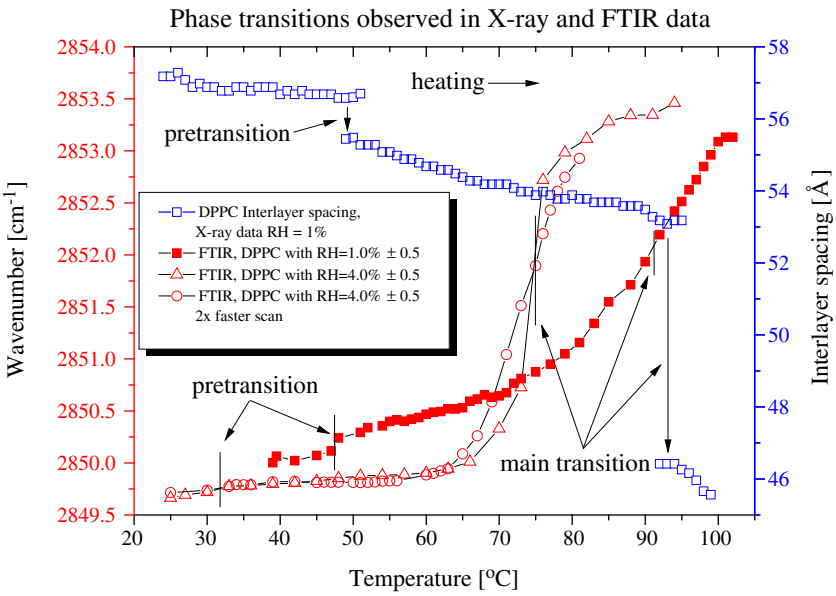

Fig. 1. The pure DPPC phase transitions observed in X-ray diffraction data and in shifts of 2850 cm^{-1} band from FTIR spectra. The main phase transition was used as a reference point to determine the multibilayers RH. The almost 5× longer measurement time in the case of X-ray data results in more dry DPPC multibilayers which is seen as a difference of ~3 °C between FTIR and X-ray data. The FTIR data circles and triangles present samples with the same RH = 4.0 but the temperature changes in the case of circle data are 2x faster which results in more smooth phase transition.

3. Results and discussion

3.1. Observed phase transition

After incorporation of XN to DPPC multibilayers a more pronounced transition in a gel phase is recorded in X-ray data. This observed transition is related to the lipid pretransition [35]. A new abbreviation of the gel lipid phases is introduced in L_I before pretransition and L_{II} after it. The reference diffraction patterns for pure DPPC multibilayers, prepared in the same way as the one with XN are presented in reference [34]. It is well-known that the main phase transition (measured using DSC) of the dry DPPC bilayer is almost 50 °C higher than for the pure lipid in the form of liposomes in water, where it reaches 41 °C [31,36]. For almost dry films the main lipid transition temperature should be around 95 °C [31,37] and has characteristic diffraction pattern, see Fig. 1. Addition of 5 mol% of XN causes shift of the lipid pretransition to around 60 °C (see, Fig. 3). At 10–20 mol% of XN this transition of L_I to L_{II} occurs around 55 °C. At these temperatures both phases coexist together. In all cases the precise values of the phase transitions are difficult to determine due to relatively weak intensities of reflections.

Because after cooling the reflexes related to the L_{II} phase do not transform to the one of the L_I phase, it suggests that XN permanently changes the lipid multibilayers properties after heating. However the XN–DPPC complex transforms at pretransition during cooling from C_{II} to C_L. In heating cycle the L_I to L_{II} phase transition occurs simultaneously with the C_I to C_{II} one.

The incorporation of XN molecules into the DPPC multibilayers caused appearance of a broader phase transition under dry conditions also in FTIR spectra. In the case of DPPC containing XN at a temperature of around 50 °C RH = 1%, there is a characteristic shift of the stretching CH_2 bands in the direction of higher frequencies. This is in compliance with the diffraction data where the observed phase transition L_I to L_{II} occurs close to this temperature (the small differences in temperature can be related to different preparation procedures between those techniques, see Materials and methods). Analysis of the positions of the stretching CH_2 bands is commonly used as a hydrocarbon chain conformation indicator [38]. The addition of XN to the pure DPPC multibilayer decreases the temperature of the pretransition and main phase transition.

3.2. XRD XN–DPPC complex observation

Fig. 2 shows X-ray scans of DPPC containing XN at different temperatures. The new structure of XN–DPPC complex indicated by reflection around $2\theta = 2.3°$ is not related to crystalline form of XN. Close to this position several substances show specific reflection that is related to the complex formation in lipid multibilayers [39]. The new reflections from DPPC–XN complex are marked with C_I and C_{II} in the figures where index $_I$ and $_{II}$ denotes two forms in a gel phase before and after pretransition. Intensity of the new reflection increase with XN concentration and its maximum measured value was observed for 20 mol% of XN (see Fig. 2 reflections C_I and C_{II}). Almost in all cases only the first order reflection form DPPC–XN complex was observed except 20 mol% of XN where second order reflection was recorded. For this XN concentration the lamellar structure of DPPC–XN complex is the most pronounced. The lamellar gel complex (C_I) has a repeat spacing of 39.8 ± 0.1 Å and in C_{II} phase 40.7 ± 0.1 Å at 63 °C. The complex thickness in the gel phase remains constant until the pretransition; however the complex in the C_{II} phase changes from 40.7 ± 0.1 to 40.2 ± 0.1 Å at 70 °C. This can be related to the water evaporation from multibilayers. The intensity of a complex reflection changes in the same fashion as the first order lipid reflection during heating, see Fig. 3. These suggest that periodic complex structure is formed during preparation not in the heating cycle. In case of 1,3,4-tiadiazole the complex formation occurs only after heating [34]. It was impossible to determine complex stoichiometry in this experiment.

3.3. Fluorescence microscopy

The fluorescence microscopy reveals precipitations in the lipid matrix after preparation. This indicates for the phase separation of the L_I and the C_I at room temperature. Area of light zones (DPPC containing significant amount of XN) increases with XN concentration (see Fig. 2). Probably the light zones contain also XN in its aggregated form.

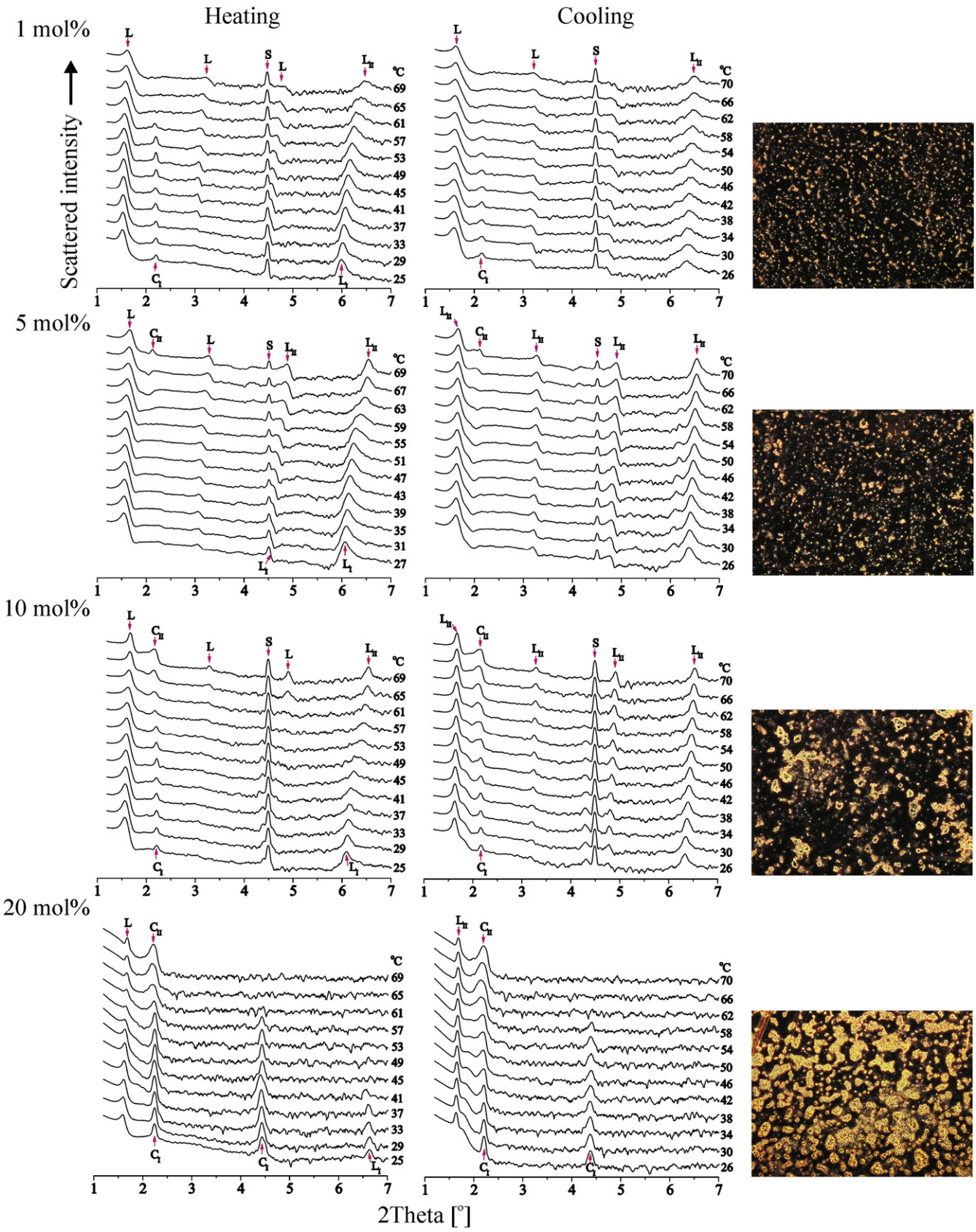

Fig. 2. Selected X-ray diffraction profiles obtained from aqueous dispersion of 1, 5, 10 and 20 mol% XN in DPPC recorded at different temperatures after drying. S stands for reflection from mica substrate, C for complex phases and L for lipid phases. In all cases a transition between 55 and 62 °C, related to the lipid pretransition, is observed. Indices $_{I}$ and $_{II}$ stand for two gel phases before and after this phase transition respectively. In case where it is impossible to distinguish reflection from lipid in gel and liquid crystal phase the L notation is used. The last two scans for 20 mol% XN are recorded on the glass plate therefore no substrate reflection is observed and the background is slightly changed. On the right is microscopic photography of the measured dry DPPC multibilayers containing XN. The pictures were taken with the Leica DM4000 fluorescence microscope in a visible light. The picture dimensions are 200 μm × 200 μm.

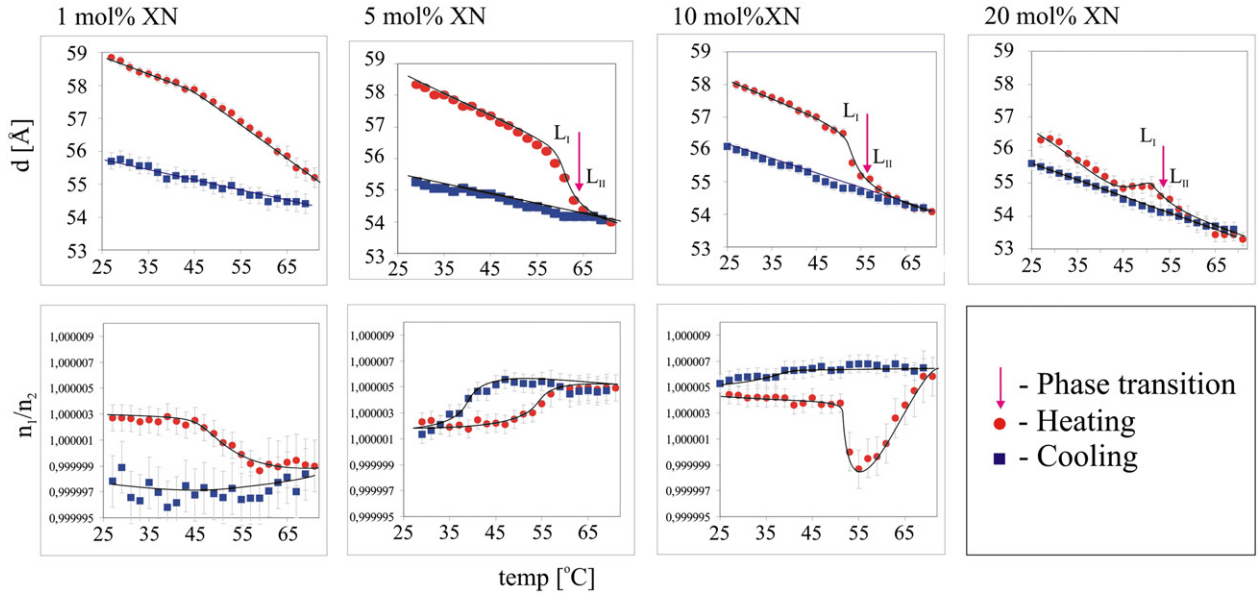

Fig. 3. The interlayer thickness and n_1/n_2 ratio in a function of temperature for concentrations: 1, 5, 10, and 20 mol% of XN. The lines are added only as guidance.

3.4. ATR-FTIR spectroscopic studies of XN—DPPC mixtures

The ATR-FTIR technique was applied with the aim of understanding the mechanisms of the molecular interactions between XN and DPPC. Fig. 4 presents ATR-FTIR spectra of the dry XN film (panel A), pure DPPC and 1, 5, 10, 20 and 50 mol% of XN in DPPC multibilayers (panel B). The most important frequencies of XN are collected in Table 1. The assignment of the fundamental vibrational bands of XN is based on literature data concerning other similar compounds [40–43]. Vibrations that have been assigned to the mutual interaction between chalcone and phospholipid are only marked in the infrared absorption spectrum of XN. In a dry XN film, the νOH band is broad and centered at around 3305 cm^{-1} as a consequence of H-bond formation by the OH groups of the chalcone molecules (also intramolecular); see Fig. 4A. After incorporation of XN into DPPC, the absorbance of this band gradually decreases except for 50 mol% of XN in DPPC (because of additional OH groups coming from XN). This effect can be related to hydrogen bonds breaking

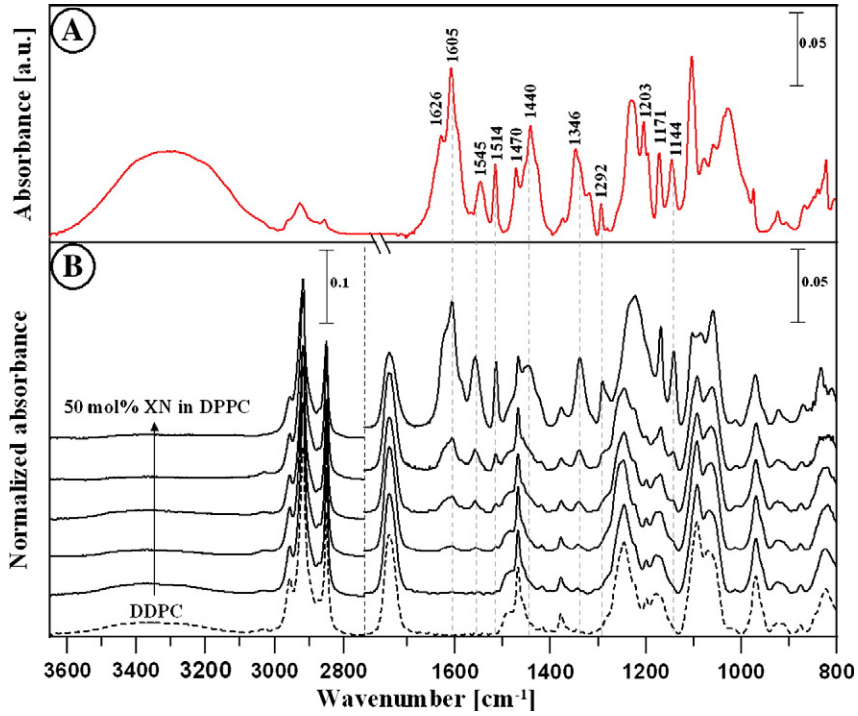

Fig. 4. The ATR-FTIR spectra of XN dissolved in methanol in the form of the dry film (panel A), from the top for 50, 20, 10, 5 and 1 mol% XN in DPPC, and pure DPPC (dashed line) at room temperature (panel B). Spectra in panel B were offset on the vertical scale for clarity and normalized by dividing by the surface beneath the bands corresponding to the overall C–H stretching vibration bands between 2800 and 3050 cm^{-1}. The multibilayers were equilibrated at 1% RH.

Table 1
Representative bands of FTIR absorbance spectra for xanthohumol and their assignment.

Wavenumber [cm^{-1}]	Vibrational assignment
974	*trans* –CH═CH–
1027	Substituted benzene
1103	
1145	ν(C–C) aromatic ring, ν(–OH)
1171	
1203	
1228	$\delta\nu$(–OH)
1292	ν(C–C) aromatic ring
1346	δ(–OH)
1440	
1470	δ(C–C)
1515	
1545	*trans* CH═CH–
1594	
1606	νC═O
1626	
2854	ν_s(–OCH_3)
2919	
2967	ν_{as} (–OCH_3)
3189	ν(–OH), ν(C–H) in aromatic ring
3393	

*ν — stretching mode, δ — bending in plane, s — symmetric vibrations, as — asymmetric vibrations,

between both lipid molecules and the lipid–XN mixture or water evaporation [44]. As can be seen from Fig. 4B, the main differences between the FTIR spectra of pure DPPC and XN—DPPC in different mole ratios involve the bands in the region characteristic for the polar head vibrations: the antisymmetric stretching of the PO_2^- groups (1246 cm^{-1}), symmetric PO_2^- stretching (1090 cm^{-1}) partially overlapping with the band representing the C–O–P–O–C stretching modes (1064 cm^{-1}) and the CH_2 scissoring mode (1467 cm^{-1}). The shape and position of these bands are especially changed at high concentration of XN in DPPC. The observed changes indicate the localization of the XN with respect to the membrane and the type of interaction with phospholipids. After incorporation of XN molecules into the lipid multibilayers no significant spectral shift of lipid main bands was observed at room temperature. The spectral shift of the shoulder centered at 1626 cm^{-1} assigned to the C═O stretching mode (coming from XN) towards lower frequencies (to 1619 cm^{-1}) indicate that XN binds to the polar part of the model membrane via hydrogen bonding between the carbonyl groups of DPPC and hydroxyl groups of XN, see Fig. 4. The weak bands at 1545 and 1514 cm^{-1} might be assigned to the –C═C– vibrations in phenol and hydroxybenzoyl moieties of XN. Interestingly, the first band mentioned is shifted towards higher frequencies by 13 cm^{-1} in DPPC. This suggests that after dispersion of XN in DPPC the Van der Waals interactions between aromatic rings in XN molecules are reduced. On the other hand, the methylene groups in the prenyl unit of XN show a possibility of rotation relative to the aromatic A-ring [18]. This part of the XN molecules could be localized in the polar–apolar interface in the lipid multibilayers in the case of high concentration of XN. The spectral shift of the band at 1440 cm^{-1} towards higher frequencies (to 1446 cm^{-1}) after incorporation of 50 mol% XN into the membranes supports the concept of chalcone localization in the membrane at the polar–nonpolar interface (after multibilayer preparation at room temperature), see Fig. 4. This can be rationalized by limited space in the polar zone of lipid bilayer. This band indicates the presence of an antisymmetric ethylenic double bond and the vibrations of choline –CH_3 group [42].

The gradual spectral shift of the band at 1346 cm^{-1} representing the C–OH deformation vibrations in XN towards lower frequencies (to 1338 cm^{-1}) suggests involvement of hydroxyl groups of the chalcone in binding via the H-bond to the lipid membrane. This effect is pronounced by the increase in the intensity of the band centered at 1144 cm^{-1} corresponding to C–OH stretching vibrations especially in the case of 20 and 50 mol% XN in DPPC.

The interaction between XN and the head group of DPPC was monitored by the PO_2^- antisymmetric stretching band, which is located at 1246 cm^{-1}, see Fig. 5A. The difference spectra obtained by subtraction of the spectrum of the dry DPPC film from the spectrum of the dry XN in the DPPC film reveal changes in the region of the lipid $\nu_{as}PO_2^-$; see Fig. 5B. As can be seen from the subtracted spectra, a new band centered around 1260 cm^{-1} appears. This band is probably related to the formation of a complex between XN and the lipid. To get better insight into the molecular interaction between XN and DPPC molecules, infrared spectra of XN dissolved in polar and non-polar solvents are presented in Fig. 5B (dotted lines). The spectrum of the dry XN film dissolved earlier in non-polar tetrachloromethane displays three bands centered at 1261, 1210 and 1191 cm^{-1} corresponding to the C–OH (non-hydrogen bonded) and C–C–H deformation vibrations in the aromatic ring [45]. In contrast, in the dry XN film dissolved earlier in methanol, two bands centered at 1227 and 1203 cm^{-1} were ascribed to the hydrogen bonded –OH groups. Interestingly, in the case of the subtracted spectra of XN in DPPC, appearance of two bands centered around 1225 and 1212 cm^{-1}, respectively, similar to hydrogen bonded XN molecules (like in methanol) and non-hydrogen bonded (like in tetrachloromethane) is gradually observed. The spectral shift of the first above-mentioned band from ~1235 to 1227 cm^{-1} is dependent on the XN concentration and involves the interaction via the H-bond between XN and the PO_2^- group in DPPC. The second band can be related to non-hydrogen bonded interactions and the possibility of organization of XN in the hydrophobic part of the model membrane.

3.5. Thermotropic phase behavior — XRD and FTIR study

Fig. 3 presents the dependence of thickness layer and refraction indices ratio n_1/n_2 as a function of temperature for DPPC mixture with 1, 5, 10 and with 20 mol% of XN. The behavior of the system during heating and cooling is different. During heating a clear transition from L_I to L_{II} in the case of lipid is observed. During cooling no phase transition indicated by X-ray diffraction is noted. This can be related to the lipid multibilayer dehydration or strong interaction between XN and DPPC or XN aggregation.

The layer thickness of L_I with 1% XN is almost the same as for pure DPPC. With the increase of the XN concentration the lipid multilayer thickness clearly decreases with minimum at 20 mol%, see Fig. 3. After heating–cooling cycle the lipid layer thickness returns in all cases to the same value of ~56 Å (the small deviations can be an effect of diffractometer alignment and/or water evaporation from multibilayers). For small concentrations of XN the repeat lipid spacing is similar to the one observed by Lenne at al. [46] but at high concentrations the situation is opposite and the lipid repeat spacing decreases with increasing XN concentration. Small dehydration was observed in FTIR spectra where after heating the band related to vibrations of hydroxyl group (3381 cm^{-1}, data not shown) decreases with temperature. This effect is well-known and widely described by reference [47]. The interlayer thickness differences after cooling are very small and cannot be correlated with the XN concentration due to small alignment differences between samples.

The multilayer thickness changes are accompanied by clear refraction changes. The n_1/n_2 ratio for 1 mol% during heating has higher value than during cooling. After 45 °C the electron density increases in lipid hydrophilic zones or decreases in hydrophilic zone but the source of these changes can be related not only to the XN but also to the carbohydrate chain ordering. In the case of 5 mol% the situation is opposite. During heating the ratio has lower value than during cooling cycle but the difference is not that pronounced. The refraction changes have hysteresis behavior with temperature. This can be explained by three possible mechanisms. In the first one, the electron

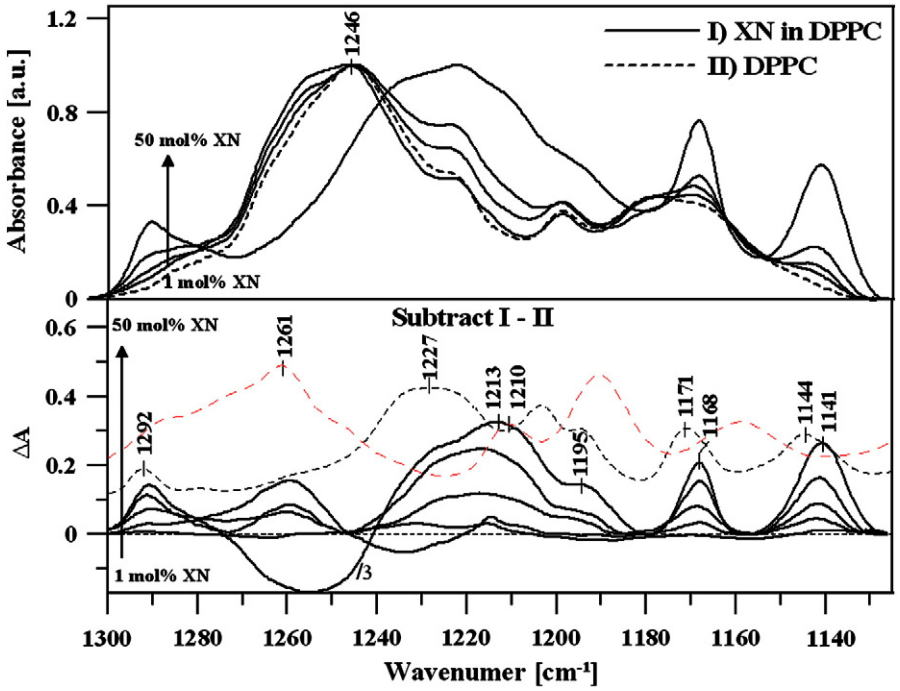

Fig. 5. (A) The region of the νPO_2^- vibrations in a dry film of XN—DPPC mixtures, from the top for, 50, 20, 10, 5 and 1 mol% XN in DPPC, and pure DPPC (dashed line). The spectra were normalized in the maximum of band centered at 1246 cm^{-1}. (B) The spectra obtained by subtraction of the spectrum of the dry DPPC film from the spectrum of the dry XN—DPPC film. Dashed lines represent infrared spectra of the dry XN film dissolved earlier in methanol (black-short dashed line) and tetrachloromethane (red-long dashed line).

density (most probably coming from XN molecules) moves to the first zone or moves in it and the ratio n_1/n_2 increases, see Fig. 5. In the second XN leaves the second zone and cumulates in aperiodic structures (invisible by X-ray diffraction e.g. XN water microphases [48] or aggregates) and in the third one XN moves between lipid zones or to the border between them. This can be rationalized as better XN dissolution in the hydrophilic lipid zones at higher temperatures for this concentration. In the case of 10 mol% the situation is similar to the one observed for 5 mol% but the phase transition is accompanied by drastic decrease of n_1/n_2 ratio during heating. It is important to mention that at pretransition the layer thickness d shrinks which is accompanied by a strong decrease of n_1/n_2 ratio. This observed effect can be partly related to the lipid zone 2 shrinking at phase transition [49], which changes the most and increase of electron density in it. The in-plane packing can follow these changes but slower, which can partly explain the changes at phase transition [50]. After pretransition the n_1/n_2 ratio and thus electron density in both layers return to the previous value which suggest that XN can incorporate/move again into zone 2 and do not change even after cooling. It is also possible that after sample heating–cooling cycle, XN molecules form associated forms (e.g. dimers, trimers and N-aggregates) which interact differently with lipid layers. At 20 mol% of XN the peaks were so broad that it was impossible to measure refraction changes from the sample. Important information about XN interaction with different lipid groups in a function of temperature provides FTIR study.

3.6. Symmetric stretching in the CH_2 vibrations

The intensive bands between 2800 and 3000 cm^{-1} represent the C–H stretching modes with the maxima of peaks at 2850 cm^{-1} and at 2917 cm^{-1}, corresponding to the symmetric and antisymmetric stretching in the CH_2 groups of alkyl chains, respectively. The vibrations of the CH_2 groups are commonly used to monitor the order–disorder state of the lipid system and consequently, to observe the lipid phase transitions [38]. The $\nu_{as}CH_2$ and ν_sCH_2 vibration modes in DPPC are diagnostic of conformational and alkyl chain packing changes [51,52]. Fig. 7 shows evaluation of frequency of the ν_sCH_2 stretching band during two subsequent heating processes with different RH. The pretransition is seen as a weak shift up of frequency around 30 °C for RH = 4% and 47 °C for RH = 1%. In this band no significant changes concerning XN lipid interactions for both presented RH values were observed except main melting transition broadening and shifting. This suggests that XN does not significantly interact with the hydrophobic part of lipid membrane.

3.7. CH_2 scissoring vibrations

Lipid hydrocarbon phase transitions can also be monitored by examining the CH_2 scissoring centered near 1467 cm^{-1}, see Fig. 7. The changes in the region corresponding to this mode are diagnostic of alkyl chain packing arrangements, as they reflect concomitant increases in hydrocarbon chain mobility and *gauche* rotamer proportion [53,54]. Position of the δCH_2 vibration is sensitive to the type of lateral alkyl chain packing [55,56]. An examination of the contours of this band at the onset of the hydrocarbon chain-melting process can provide useful information about the intermolecular interaction. In a gel phase, this band is relatively sharp and intensive, indicating hexagonal packing. With increasing temperature the intensity of the δCH_2 band decreases, becomes broader and the center of the band shifts in the direction of lower frequencies, see Fig. 7. These mentioned observations indicate for a loss of hexagonal chain order. Additionally the band initially observed at frequencies near 1467 cm^{-1} begins to be shifted to a lower-frequency region after main phase transition for both 1% and 4% RH. The small changes around 33 °C and 48 °C for RH = 4 and 1% respectively, can indicate for in-plane reorganization of hydrocarbon chains close to the lipid pretransition which can be correlated with interlayer spacing changes observed in X-ray measurements. For all concentrations of XN the changes in this band are similar for both RH values.

3.8. PO_2^- antisymmetric vibrations

The most important bands for probing directly the head group of DPPC interactions with XN is the PO_2^- antisymmetric stretching mode, which is located around 1246 cm^{-1} and symmetric stretching mode which is located around 1090 cm^{-1}. Both bands show the same behavior with temperature therefore only the second one will be presented. This band is the most sensitive to the formation of H-bonds, shifting to lower frequencies with increased H-bonding [57]. In a dry DPPC film, it is centered at 1092 cm^{-1}. However, in comparison to multibilayer containing XN observed changes in the band position in the investigated temperature range are minor, see Fig. 7. Increase of the temperature close to the pretransition for RH = 4% causes shift of this band position towards lower frequencies which indicates a strong interaction via hydrogen bonds between the PO_2^- group of the lipid and the OH groups of XN, see Fig. 6. After that the band frequency shifts to higher values. This effect is observed for all investigated XN concentrations. After second heating the band does not change at pretransition and at main transition goes down. This suggests that after first heating XN molecules changed or formed different forms that do not interact with DPPC like the XN from newly prepared samples. This is with accordance with X-ray data where after cooling for all concentrations of XN no changes are observed.

3.9. C═O stretching vibrations

The temperature dependence of the frequency of the C═O stretching modes of DPPC multibilayers in the XN is shown in Fig. 7. In the DPPC film with RH = 4%, the band of ν C═O is centered around 1737.5 cm^{-1} and is stable in the 25 to 70 °C temperature range. In the presence of XN molecules, a minor lower frequency shift of the ν C═O group vibrations is observed at pretransition. These changes are similar to the one observed in the case of PO_2^- group but with much smaller amplitude which suggests that XN at this temperature interacts more selectively with PO_2^- groups and only partly with the C═O one, see Fig. 5. The hydrogen bonding may occur between oxygen atoms in the C═O groups of lipid and hydrogen in the OH group of XN. At temperature above the main melting transition, a shift to a higher-frequency region (see, Fig. 7) is observed and the contour of this band broadens (spectra not shown). In the second heating cycle the band behaves differently than for pure DPPC. Above 90 °C this band goes down which suggests that at this temperature XN–DPPC system becomes unstable. This is with compliance with X-ray data where the lipid layers at this temperature are partly damaged.

3.10. $N^+(CH_3)_3$ asymmetric vibration

A study of the asymmetric $N^+(CH_3)_3$ stretching mode shows more pronounced changes for RH = 4% for all measured multibilayers containing XN than for the pure DPPC at pretransition, see Fig. 7. This is with accordance with presented model in Fig. 5 where firstly XN moves in the direction of PO_2^- at pretransition and than the interactions in hydrophilic lipid zone after layer shrinking becomes more pronounced. The band frequency goes faster down than the one of pure DPPC for all measured XN–DPPC multibilayers. This can be related to the layer shrinking and stronger interaction between groups in hydrophilic zone of lipid. In a second heating cycle a permanent lowering of this band frequency is observed which suggests that the XN–DPPC system is irreversibly changed.

4. Conclusions

We have presented the interaction of the major prenylated chalcone xanthohumol with DPPC in the form of dry multibilayers. The incorporation of XN inside such a lipid system model has an influence on the molecular organization and the structural properties in a polar part of lipid bilayers. It was found that XN is located in interface region between polar heads of lipids and at pretransition moves close to the PO_2^- groups. After that XN cumulates outside of periodic lipid structure which is seen in permanent change of lipid layer thickness and permanent change of FTIR frequency position in second heating cycle for phosphate groups. These changes are even more pronounced at higher concentrations of XN. The effect of XN on multibilayer net is to decrease interlayer spacing and the decrease of the temperature of the main lipid transition for RH = 1 and 4%. It was found that DPPC multibilayers decompose/change above ~75 °C at RH = 1%. The results obtained show the possibility of forming the XN—DPPC complex. Already at 1 mol% of XN, a complex XN—DPPC is observed, which has also lamellar structure like lipids. It is noteworthy that for the first time we have presented X-ray diffraction and spectroscopic of pure xanthohumol and xanthohumol in DPPC multibilayers at different concentrations and RH values of 1% and 4%.

Acknowledgements

This research was financed by National Science Center of Poland within the research project no. N N209 0324 40.

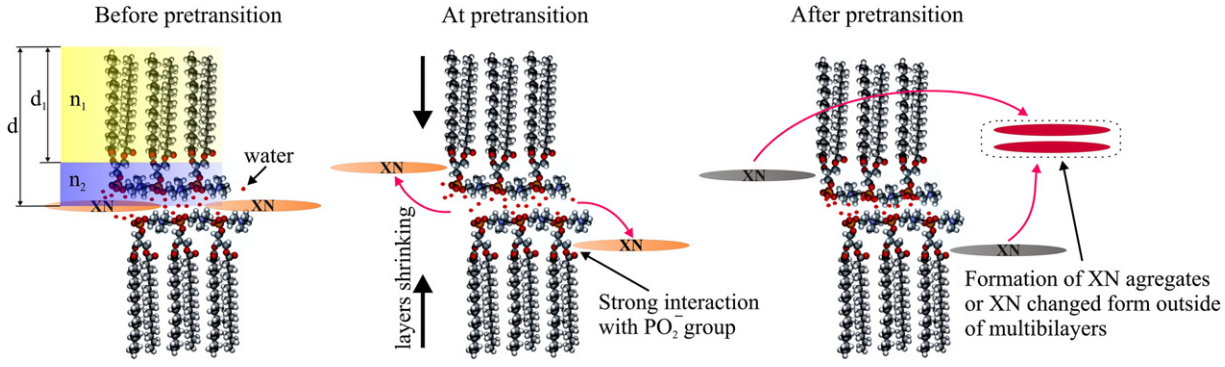

Fig. 6. The most probable mechanism which explains the thermotropic changes observed in X-ray and FTIR data. Before pretransition XN is located between hydrophilic zones of DPPC. At pretransition XN moves close to the interfacial part of lipid. This is seen in X-ray data as a strong decrease of n_1/n_2 ratio and frequency decrease of PO^{2-} band. After pretransition the lipid interlayer spacing is smaller and the interaction with PO^{2-} becomes weaker. Very weak changes in CH_2 bands indicate for the weak interaction of XN with this group. Subsequent cooling and heating do not bring any significant changes to the system.

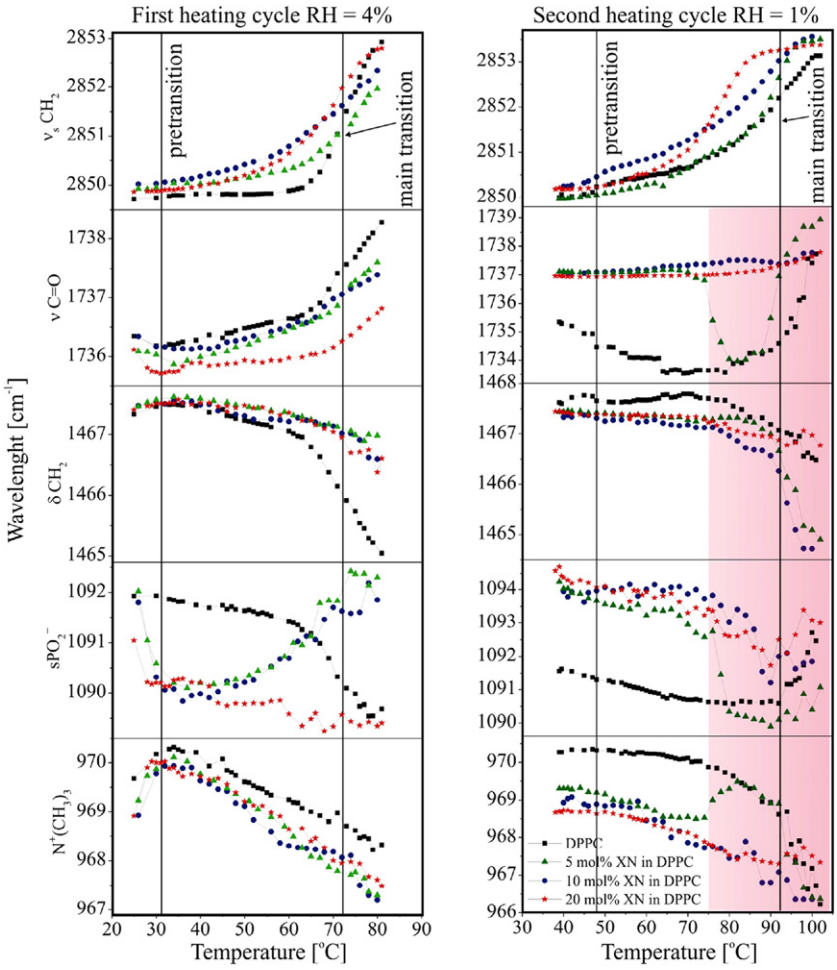

Fig. 7. Temperature-dependent FTIR changes in the DPPC multibilayers containing XN for the first heating (RH = 4% ± 0.5) and second heating cycle (RH = 1% ± 0.3). In the second cycle the area above 75 °C shows data with high error bars related to the peak broadening and partial DPPC decomposition. The vertical lines show phase transitions for DPPC.

References

[1] J.F. Stevens, A.W. Taylor, J.E. Clawson, M.L. Deinzer, Fate of xanthohumol and related prenylflavonoids from hops to beer, J. Agric. Food Chem. 47 (1999) 2421–2428.

[2] C. Dorn, J. Heilmann, C. Hellerbrand, Protective effect of xanthohumol on toxin-induced liver inflammation and fibrosis, Int. J. Clin. Exp. Pathol. 5 (2012) 29–36.

[3] J.F. Stevens, J.E. Page, Xanthohumol and related prenylflavonoids from hops and beer: to your good health! Phytochemistry 65 (2004) 1317–1330.

[4] C.L. Miranda, Y.H. Yang, M.C. Henderson, J.F. Stevens, G. Santana-Rios, M.L. Deinzer, D.R. Buhler, Prenylflavonoids from hops inhibit the metabolic activation of the carcinogenic heterocyclic amine 2-amino-3-methylimidazo[4, 5-f]quinoline, mediated by cDNA-expressed human CYP1A2, Drug Metab. Dispos. 28 (2000) 1297–1302.

[5] Y. Wang, Y. Chen, J. Wang, J. Chen, B.B. Aggarwal, X. Pang, M. Liu, Xanthohumol, a prenylated chalcone derived from hops, suppresses cancer cell invasion through inhibiting the expression of CXCR4 chemokine receptor, Curr. Mol. Med. 12 (2012) 153–162.

[6] T.L. Yen, C.K. Hsu, W.J. Lu, C.Y. Hsieh, G. Hsiao, D.S. Chou, G.J. Wu, J.R. Sheu, Neuroprotective effects of xanthohumol, a prenylated flavonoid from hops (*Humulus lupulus*), in ischemic stroke of rats, J. Agric. Food Chem. 60 (2012) 1937–1944.

[7] C. Gerhauser, A. Alt, E. Heiss, A. Gamal-Eldeen, K. Klimo, J. Knauft, I. Neumann, H.R. Scherf, N. Frank, H. Bartsch, H. Becker, Cancer chemopreventive activity of xanthohumol, a natural product derived from hop, Mol. Cancer Ther. 1 (2002) 959–969.

[8] S. Monteghirfo, F. Tosetti, C. Ambrosini, S. Stigliani, S. Pozzi, F. Frassoni, G. Fassina, S. Soverini, A. Albini, N. Ferrari, Antileukemia effects of xanthohumol in Bcr/Abl-transformed cells involve nuclear factor-kappaB and p53 modulation, Mol. Cancer Ther. 7 (2008) 2692–2702.

[9] R. Monteiro, C. Calhau, A.O. Silva, S. Pinheiro-Silva, S. Guerreiro, F. Gartner, I. Azevedo, R. Soares, Xanthohumol inhibits inflammatory factor production and angiogenesis in breast cancer xenografts, J. Cell. Biochem. 104 (2008) 1699–1707.

[10] B. Vanhoecke, L. Dolle, A. Vercoutter-Edouart, J. Antol, H. Depypere, M. Bracke, A proteomic approach to understand the anti-invasive and pro-apoptotic effect of xanthohumol in human breast cancer cells, Mol. Cell. Proteomics 4 (2005) S57-S57.

[11] C.L. Miranda, J.F. Stevens, A. Helmrich, M.C. Henderson, R.J. Rodriguez, Y.H. Yang, M.L. Deinzer, D.W. Barnes, D.R. Buhler, Antiproliferative and cytotoxic effects of prenylated flavonoids from hops (*Humulus lupulus*) in human cancer cell lines, Food Chem. Toxicol. 37 (1999) 271–285.

[12] M.C. Henderson, C.L. Miranda, J.F. Stevens, M.L. Deinzer, D.R. Buhler, In vitro inhibition of human P450 enzymes by prenylated flavonoids from hops, *Humulus lupulus*, Xenobiotica 30 (2000) 235–251.

[13] Q. Wang, Z.H. Ding, J.K. Liu, Y.T. Zheng, Xanthohumol, a novel anti-HIV-1 agent purified from hops *Humulus lupulus*, Antiviral Res. 64 (2004) 189–194.

[14] E.C. Colgate, C.L. Miranda, J.F. Stevens, T.M. Bray, E. Ho, Xanthohumol, a prenylflavonoid derived from hops induces apoptosis and inhibits NF-kappaB activation in prostate epithelial cells, Cancer Lett. 246 (2007) 201–209.

[15] J.F. Stevens, A.W. Taylor, M.L. Deinzer, Quantitative analysis of xanthohumol and related prenylflavonoids in hops and beer by liquid chromatography–tandem mass spectrometry, J. Chromatogr. A 832 (1999) 97–107.

[16] F.B. Power, F. Tutin, H. Rogerson, The constituents of hops, J. Chem. Soc. 103 (1913) 1267–1292.

[17] M. Vandewalle, On the synthesis of xanthohumol and isoxanthohumol, Bull. Soc. Chim. Belg. 70 (1961) 163–167.

[18] L.R. Chadwick, D. Nikolic, J.E. Burdette, C.R. Overk, J.L. Bolton, R.B. van Breemen, R. Frohlich, H.H. Fong, N.R. Farnsworth, G.F. Pauli, Estrogens and congeners from spent hops (*Humulus lupulus*), J. Nat. Prod. 67 (2004) 2024–2032.

[19] M. Yilmazer, J.F. Stevens, M.L. Deinzer, D.R. Buhler, In vitro biotransformation of xanthohumol, a flavonoid from hops (*Humulus lupulus*), by rat liver microsomes, Drug Metab. Dispos. 29 (2001) 223–231.

[20] A. Semalty, M. Semalty, D. Singh, M.S.M. Rawat, Preparation and characterization of phospholipid complexes of naringenin for effective drug delivery, J. Incl. Phenom. Macrocycl. Chem. 67 (2010) 253–260.

[21] H. Hirata, K. Takazumi, S. Segawa, Y. Okada, N. Kobayashi, T. Shigyo, H. Chiba, Xanthohumol, a prenylated chalcone from *Humulus lupulus* L., inhibits cholesteryl ester transfer protein, Food Chem. 134 (2012) 1432–1437.

[22] A. Arora, T.M. Byrem, M.G. Nair, G.M. Strasburg, Modulation of liposomal membrane fluidity by flavonoids and isoflavonoids, Arch. Biochem. Biophys. 373 (2000) 102–109.

[23] P.I. Oteiza, A.G. Erlejman, S.V. Verstraeten, C.L. Keen, C.G. Fraga, Flavonoid–membrane interactions: a protective role of flavonoids at the membrane surface? Clin. Dev. Immunol. 12 (2005) 19–25.
[24] B. Pawlikowska-Pawlega, L.E. Misiak, B. Zarzyka, R. Paduch, A. Gawron, W.I. Gruszecki, Localization and interaction of genistein with model membranes formed with dipalmitoylphosphatidylcholine (DPPC), Biochim. Biophys. Acta 1818 (2012) 1785–1793.
[25] H.A. Scheidt, A. Pampel, L. Nissler, R. Gebhardt, D. Huster, Investigation of the membrane localization and distribution of flavonoids by high-resolution magic angle spinning NMR spectroscopy, Biochim. Biophys. Acta 1663 (2004) 97–107.
[26] A. Saija, F. Bonina, D. Trombetta, A. Tomaino, L. Montenegro, P. Smeriglio, F. Castelli, Flavonoid–biomembrane interactions — a calorimetric study on dipalmitoylphosphatidylcholine vesicles, Int. J. Pharm. 124 (1995) 1–8.
[27] R. Sihna, M.K. Gadhwal, U.J. Joshi, S. Srivastava, G. Govil, Modifying effect of quercetin on model biomembranes: studied by molecular dynamic simulation, DSC and NMR, Int. J. Curr. Pharm. Res. 4 (2012) 70–79.
[28] C. van Dijk, A.J.M. Driessen, K. Recourt, The uncoupling efficiency and affinity of flavonoids for vesicles, Biochem. Pharmacol. 60 (2000) 1593–1600.
[29] H. Tsuchiya, M. Nagayama, T. Tanaka, M. Furusawa, M. Kashimata, H. Takeuchi, Membrane-rigidifying effects of anti-cancer dietary factors, Biofactors 16 (2002) 45–56.
[30] Y.S. Tarahovsky, E.N. Muzafarov, Y.A. Kim, Rafts making and rafts braking: how plant flavonoids may control membrane heterogeneity, Mol. Cell. Biochem. 314 (2008) 65–71.
[31] M. Kodama, M. Kuwabara, S. Seki, Successive phase-transition phenomena and phase-diagram of the phosphatidylcholine–water system as revealed by differential scanning calorimetry, Biochim. Biophys. Acta 689 (1982) 567–570.
[32] W. Pohle, C. Selle, H. Fritzsche, H. Binder, Fourier transform infrared spectroscopy as a probe for the study of the hydration of lipid self-assemblies. I. Methodology and general phenomena, Biospectroscopy 4 (1998) 267–280.
[33] J. Xiaoming, W. Ziqin, Bragg's law with refractive correction of low-angle X-ray diffraction for periodic multilayers, Chin. Phys. Lett. 8 (1991) 356.
[34] D.M. Kaminski, A. Matwijczuk, D. Pociecha, E. Gorecka, A. Niewiadomy, M. Dmowska, M. Gagoś, Effect of 2-(4-fluorophenylamino)-5-(2,4-dihydroxyphenyl)-1,3,4-thiadiazole on the molecular organisation and structural properties of the DPPC lipid multibilayers, Biochim. Biophys. Acta 118 (2012) 2850–2859.
[35] T. Heimburg, A model for the lipid pretransition: coupling of ripple formation with the chain-melting transition, Biophys. J. 78 (2000) 1154–1165.
[36] K. Ciesik, A. Koll, J. Grdadolnik, Structural characterization of a phenolic lipid and its derivative using vibrational spectroscopy, Vib. Spectrosc. 41 (2006) 14–20.
[37] Z.V. Leonenko, E. Finot, H. Ma, T.E. Dahms, D.T. Cramb, Investigation of temperature-induced phase transitions in DOPC and DPPC phospholipid bilayers using temperature-controlled scanning force microscopy, Biophys. J. 86 (2004) 3783–3793.
[38] T. Le Bihan, M. Pe'zolet, Study of the structure and phase behavior of dipalmitoylphosphatidylcholine by infrared spectroscopy: characterization of the pretransition and subtransition, Chem. Phys. Lipids 94 (1998) 13–33.
[39] X. Wang, P.J. Quinn, The structure and phase behaviour of alpha-tocopherol-rich domains in 1-palmitoyl-2-oleoyl-phosphatidylethanolamine, Biochimie 88 (2006) 1883–1888.
[40] O. Unsalan, A. Yilmaz, O. Bolukbasi, B. Ozturk, H.H. Esenoglu, G.O. Ildiz, C.Y. Ornek, Micro-Raman, FTIR, SEM–EDX and structural analysis of the Canakkale meteorite, Spectrochim. Acta A Mol. Biomol. Spectrosc. 92 (2012) 250–255.
[41] B.T. Ngadjui, J. Watchueng, F. Keumedjio, B. Ngameni, I.K. Simo, B.M. Abegaz, Prenylated chalcones, flavone and other constituents of the twigs of *Dorstenia angusticornis* and *Dorstenia barteri* var. *subtriangularis*, Phytochemistry 66 (2005) 687–692.
[42] M. Khalilullah, V.M. Sharma, P.S. Rao, K.R. Raju, Crotaramosmin, a new prenylated flavanone from *Crotalaria ramosissima*, J. Nat. Prod. 55 (1992) 229–231.
[43] N. Tabata, M. Ito, H. Tomoda, S. Omura, Xanthohumols, diacylglycerol acyltransferase inhibitors, from *Humulus lupulus*, Phytochemistry 46 (1997) 683–687.
[44] H. Binder, O. Zschornig, The effect of metal cations on the phase behavior and hydration characteristics of phospholipid membranes, Chem. Phys. Lipids 115 (2002) 39–61.
[45] O. Unsalan, Y. Erdogdu, M.T. Gulluoglu, FT-Raman and FT-IR spectral and quantum chemical studies on some flavonoid derivatives: Baicalein and Naringenin, J. Raman Spectrosc. 40 (2009) 562–570.
[46] T. Lenne, C.J. Garvey, K.L. Koster, G. Bryant, Kinetics of the lamellar gel–fluid transition in phosphatidylcholine membranes in the presence of sugars, Chem. Phys. Lipids 163 (2010) 236–242.
[47] N.Y. Ryabova, M.A. Kiselev, A.I. Beskrovnyi, A.M. Balagurov, Investigation of the structure of multilayer lipid membranes by real-time neutron diffraction, Phys. Solid State 52 (2010) 1050–1058.
[48] T. Lenne, G. Bryant, C.J. Garvey, U. Kelderling, K.L. Koster, Location of sugars in multilamellar membranes at low hydration, Physica B 385–86 (2006) 862–864.
[49] S. Barman, N.V. Venkataraman, S. Vasudevan, R. Seshadri, Phase transitions in the anchored organic bilayers of long-chain alkylammonium lead iodides (CnH2n + 1NH3)(2)PbI4; n = 12, 16, 18, J. Phys. Chem. B 107 (2003) 1875–1883.
[50] H. Nagase, H. Ueda, M. Nakagaki, Temperature change of the lamellar structure of DPPC/disaccharide/water systems with low water content, Biochim. Biophys. Acta Biomembr. 1371 (1998) 223–231.
[51] V.R. Kodati, M. Lafleur, Comparison between orientational and conformational orders in fluid lipid bilayers, Biophys. J. 64 (1993) 163–170.
[52] V.R. Kodati, R. Eljastimi, M. Lafleur, Contribution of the intermolecular coupling and librotorsional mobility in the methylene stretching modes in the infrared-spectra of acyl chains, J. Phys. Chem. 98 (1994) 12191–12197.
[53] R. Mendelsohn, D.J. Moore, Vibrational spectroscopic studies of lipid domains in biomembranes and model systems, Chem. Phys. Lipids 96 (1998) 141–157.
[54] H. Chen, R. Mendelsohn, M.E. Rerek, D.J. Moore, Fourier transform infrared spectroscopy and differential scanning calorimetry studies of fatty acid homogeneous ceramide 2, Biochim. Biophys. Acta 1468 (2000) 293–303.
[55] F.G. Wu, Q. Jia, R.G. Wu, Z.W. Yu, Regional cooperativity in the phase transitions of dipalmitoylphosphatidylcholine bilayers: the lipid tail triggers the isothermal crystallization process, J. Phys. Chem. B 115 (2011) 8559–8568.
[56] R.N.A.H. Lewis, R.N. McElhaney, in: A.M. Dopico (Ed.), Methods in Molecular Biology, vol. 400, Humana Press, Totowa, NJ, 2007, pp. 207–226.
[57] R.N.A.H. Lewis, R.N. McElhaney, The structure and organization of phospholipidbilayers as revealed by infrared spectroscopy, Chem. Phys. Lipids 96 (1998) 9–21.